Research Square

Preprints are preliminary reports that have not undergone peer review.
They should not be considered conclusive, used to inform clinical practice,
or referenced by the media as validated information.

Dual-Core Photonic Crystal Fiber Integrated SPR Sensor and Polarization Filter Based on Coupled Mode Theory

Jawad khan
Yanshan University
Hailiang chen
hlchen@ysu.edu.cn
Yanshan University
Sajid Ullah
Beijing Institute of Technology
Tong Zhang
Yanshan University
Aiyandrilla Dutta
Yanshan University
Sa Zhang
Yanshan University
Junling Hu
Yanshan University
Chunhao Yin
Yanshan University

Research Article

Keywords: photonic crystal fiber, optical fiber sensor, surface plasmon resonance, refractive index sensor, polarization filtering, finite elements model

Posted Date: May 19th, 2026

DOI: https://doi.org/10.21203/rs.3.rs-9555842/v1

License: This work is licensed under a Creative Commons Attribution 4.0 International License.
Read Full License

Additional Declarations: No competing interests reported.

Version of Record: A version of this preprint was published at Plasmonics on October 9th, 2026. See the published version at https://doi.org/10.1007/s11468-026-03426-9.

Dual-Core Photonic Crystal Fiber Integrated SPR Sensor and Polarization Filter Based on Coupled Mode Theory

Jawad khan[1] . Hailiang Chen[1, *]. Sajid Ullah[2] . Tong Zhang[1] . Aiyandrilla Dutta[1] . Sa Zhang[1] . Junling Hu[1] . Chunhao Yin[1]

[1] State Key Laboratory of Metastable Materials Science & Technology and Key Laboratory for Microstructural Materials Physics of Hebei Province, School of Science, Yanshan University, Qinhuangdao 066004, China.

[2] Beijing Engineering Research Center of Mixed Reality and Advanced Display, School of Optics and Photonics, Beijing Institute of Technology, Beijing 100081, China

✉ Corresponding Email: hlchen@ysu.edu

Keywords: photonic crystal fiber, optical fiber sensor, surface plasmon resonance, refractive index sensor, polarization filtering, finite elements model.

Abstract

Based on coupled mode theory, we propose a dual-polished photonic crystal fiber (PCF) with a surface plasmon resonance (SPR) and a polarizing filter, and demonstrate its design using numerical simulations. A polished gold (Au) coated surface and a dual core optimize the interaction between light and matter. A thin gold film was deposited onto the polished corners of the sensor's cladding regions in order to calculate its refractive index (RI). Based on the finite element method (FEM) implemented in the COMSOL Multiphysics software, the performance of the photonic crystal fiber sensor was carefully analyzed. It demonstrated excellent performance in measuring the refractive index of various analytes with refractive indexes of 1.30 to 1.40, with a wavelength sensitivity (WS) of 8800 nm/RIU, a spectral resolution of $1.13636\times10^{-5}$and an amplitude sensitivity (AS) of 286 RIU^{-1}. When the refractive index of the analyte is 1.37, the maximum confinement loss for the Y-polarized odd mode is 143,160 dB/m. The polarization filter effect showed an extinction ratio of -65.85 dB at a propagation distance of 2 mm, which is considered good. Its simplicity and cost-effectiveness make this design superior to existing standards. The structure can detect various analytes, thus having high flexibility in practical applications such as biosensors and integrated photonic systems.

Introduction

Surface plasmon resonance (SPR) technology has gained lots of attention in recent years due to its excellent sharpness and extensive use in food safety [1] , chemical detection [2], environmental monitoring, and biological detection [3-4]. The earliest optical fiber SPR devices used a prism coupling model based on diminished complete meditation. The Kretschmann [5] and Otto type [6] are types of SPR prisms. Among them, the Kretschmann type is the most commonly used. In terms of prism coupling models, there are two drawbacks. Measurements with SPR are only suitable for long ranges and large sizes [7]. The SPR signal was readily influenced by mechanical structures and light source variations as a result.

A novel sensor is being developed to overcome these shortcomings and enhance efficiency. SPR sensors at the micron level are constructed using fiber optics, rather than prisms. Traditional optical fibers had less ability to regulate characteristics, transmission of light, such as loss of transmission, spectrum sensitivity, and transmission mode [8-9]. Photonic crystal fiber (PCF) has many advantages over traditional optical fiber, including controllable chromatic dispersion, high birefringence, and endless single-mode transmission [10-11]. PCF-based SPR sensor perfectly achieves the light performance of the device. Optical sensors increase the efficiency of optical computing, signal processing, and communication networks. The technology has many advantages over additional optical and electrical

devices, such as reduced signal distortion, smaller size, lower cost, immune to electrical interference, and faster potential speeds. In the last few years, surface plasmon resonance (SPR) technology has significantly improved sensors, absorbers, and solar cells [12]. SPR gained more attention due to these applications.

Metal-dielectric interfaces generate the collective oscillations by interacting with free electrons and photons. Whenever a phase evanescent wave coincides with SPPs, the SPR is excited. The loss spectrum shows a sharp peak of resonance as the SPR occurs. As a result, the wavelength and resonant peak related to the refractive index (RI) of the analyte are lost [14]. SPR technology usually involves both internal and external analyte sensor mechanisms. External analytes are positioned on the outside of the fiber structure. Analytes filled air holes inside the structure of fiber for internal analyte detection [13-14]**.** But it is impossible to be done in experimental, because the analyte must be changed many times in the experiment, so it is hard to empty and fill up the air holes. To the internal sensing and external using the analyte method could be created to get the issue around the internal sensing. It is a more popular method for the detection and implementation approach.

The strongly coupled mode allows for efficient energy exchange between cores, making the fiber highly sensitive to external changes and enabling sensing. The wavelength dependence of this coupling allows for the selective blocking of specific modes, which is essential for filtering. This interaction results in a high extinction coefficient, providing clearer signals and more precise measurements. The fundamental basis for polarization is the coupling theory [15]. The polarization of splitters also allows the light in one axis, in the Y-axis or X-axis, for a particular purpose and blocks the other axis, is one of the important components of an optical integrated circuit. The limited use of traditional sensor together with restricted function due to their large size and uses, consisted shortcoming needed to be solved. Over time, sensor technology is growing due to technological advancement and researchers' efforts.

The most common plasmonic material are silver [16], gold [17], graphene [18] and copper. Gold is a great choice due to its large displacement of resonant wavelength, corrosion resistance, biocompatibility and also its stable chemical properties. Silver can be achieved sharper resonant peak. Silver is easily oxidized in a humid environment, so it can reduce the sensing performance [19]. As compare to the gold and silver the graphene and copper a susceptible of oxidation [20] .

The literature describes several types of SPR manufacturing sensors, including U-shaped SPR fiber optic sensors and tapered SPR sensors [21]. It consists of dual shaped SPR sensor; furthermore, the development of this technology in development is continuing [22-23].Due to the simplicity of the preparing methodology, the smooth polishing of the surface of the fiber is the most suitable and convenient material for sketch nanoparticle and nanostructure sensors.

In recent years, surface plasmon polaritons (SPPs) generated by specific polarization excitation have been used to modulate the refractive index. Lu et al. In 2018, we introduced the Au -grating PCF-SPR sensor with a resolution of 5.98×10^{-6} and a WS of 3340 nm/RIU for analytes in the RI range of 1.36–1.38 [24]. In 2024, Sajid Ullah et al. developed a sensor using analytes with a refractive index (RI) ranging from 1.30 to 1.40. Numerical calculations indicate that the wavelength sensitivity (WS) is expected to be 9400 nm/RIU, the amplitude sensitivity (AS) is 27.27 RIU^{-1}, and the spectral wavelength resolution is 1.063×10^{-5} [1]. In 2015, Chen et al. proposed an ultra-wideband polarization filter based on a D-shaped PCF sensor. The obtained ER was less than -20 dB, which was considered more favorable with respect to polarization effects [25].In 2021 Li et al The outside of the PCF was coated with a gold film. The detection range of the RI analyzer was 1.33–1.41. For even and odd values, the maximum sensitivity was 8500 nm RIU^{-1}, 8400 nm RIU^{-1}, respectively [7]. Sa Zhang et al, in 2023, proposed A plasmonic refractive index sensor with a broad measurement interval using a photonic crystal fiber side-polished. The designed refractive index sensor boasts a maximum sensitivity of 14600 nmRIU-1 and an extremely broad measurement range of 1.20 to 1.38 [26]. In 2019, Yu et al. sketched an Au-plated sensor of D-type SCF refractive index based on SPR, demonstrating sensitivity to RIU-1 at 2650 nm with a range of 1.25–1.6 refractive index detection[27].

Our study presents a gold (Au) dual-function surface plasmon resonance sensor and polarization filter in dual core photonic crystal fiber based on a strong mode coupling in dual-core photonic crystal fiber. Two Quincunx-shaped air holes are the innovative feature of this structure, which involves the use of strongly coupled modes among the dual cores. A plasmonic material is considerably more likely to communicate with guided light when this is achieved. Coated gold (Au) is often used as a plasmonic material in contact with analytes. Dual-function sensing is achieved by using different resonance properties of gold (Au) and different polarization directions. As a result of the optimization of the structure in the analyte range of 1.30-1.40, the maximum WS wavelength sensitivty of 8800 nm/RIU can be obtained, with an analyte RI of 1.37; the maximum confinement loss is predicted to be 143,160 dB/m is for Y-polarization odd mode. The extinction ratio for polarization filter effect is -65.85 dB, a spectral resolution of 1.13636 and the amplitude sensitivity (AS) 286 RIU^{-1}. A low-cost and easy-to-fabricate sensor, compared with those described in the literature.

Sensing Model and Method

Two-dimensional and three-dimensional cross-sectional views of the PCF-SPR sensor are shown in Figure 1, respectively. Simulations were performed using COMSOL Multiphysics software, and numerical analysis was executed to enhance (FEM) the finite element method. For the boundary, we used the perfectly matched layer (PML) method to calculate the properties of the sensors guiding. The fig. 1 (a) showing three different type of air holes d_1=0.70 µm two near with upper channel and two with bottom, d_2=0.40 µm in the center and the ten air holes arranged in two shape of Quincunx d_3=0.60 µm with spacing of Λ_1=1 µm, and depth polishing is from 0.44 to 0.71 µm, analyte thickness from 0.31 to 0.71 µm, Au thickness of 0.4 µm, the variation of PML thickness is from 0.7 to 1.5 µm, and the cladding diameter is 9.7 µm.

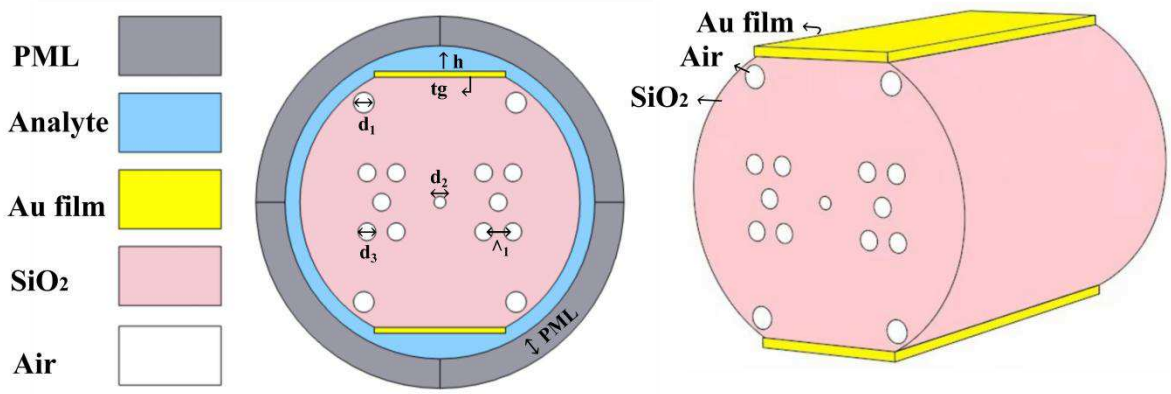


Figure.1 PCF-SPR sensor Two-dimension and Three-dimension structure.

The background material silica is fused, and the following Sellmeier equation, as shown in equation (1), is used to determine the refractive index (RI). Light wavelength represented by λ, its unit is µm, and *n* is representing the refractive index of fused silica.

$$n^2=1+\frac{0.6961663\lambda^2}{\lambda^2-(0.0684043)^2}+\frac{0.4079426\lambda^2}{\lambda^2-(0.11622414)^2}+\frac{0.8974794\lambda^2}{\lambda^2-(9.86161)^2} \quad (1)$$

To solve this problem, a Lorentz term must be added, since the dielectric constant of gold is much lower than that of silver or aluminum. However, the techniques of the model are suited to the Drude-Lorentz model. The advantage, compared to the Drude model, of offering a smaller margin of error over a wider spectral range. The Drude-Lorentz model can be used to determine the dielectric constant of Au as follows:

$$\varepsilon_m=\varepsilon_\infty - \frac{\omega_D^2}{\omega(\omega-j\gamma_D)} - \frac{\Delta_\varepsilon}{(\omega^2-\Omega_L^2)-j\Gamma_L\omega} \quad (2)$$

At high frequency the dielectric constant is (ε_∞ = 59.673) epresented as ε_∞ , ε_m is the metal's dielectric and the light angular frequency is represented by ω. The Damping frequency is γ_D(γ_D=31.84π THz) and ω_D(ω_D=4227.2π) THz is the plasma frequency. The weighting factor is representing by Δ_ε(Δ_ε=1.09). Frequency of Lorentz oscillator is denoted as Ω_L(Ω_L=1300.14π THz) and the spectral width is Γ_L(Γ_L=209.72 π THz). when core mode matches the phase of the surface plasmon polariton (SPP) mode, this effect excites the (SSP) mode. At this point, the SPP mode easily absorbs energy transferred from the core mode, causing its energy to increase while the energy of the core mode more quickly decreases. The limiting loss of the transmission mode is an intuitive parameter of detection performance. It depends on the wavelength of the light and the imaginary(n_{eff}) part of the effective refractive index, and can be expressed as follows:∞

$$\alpha\ (\mathrm{dB}cm^{-1})=8.686\times\frac{2\pi}{\lambda}\ \mathrm{Im}\ (n_{eff})\times10^4 \quad (3)$$

This is n_{eff} imaginary part and this is Im(n_{eff}) the confinement loss operating wavelength is represented by α, λ and Im(n_{eff}).

The coated area with metal is the main sensing area, RI on the both sides due to their change the result variation of, n_{eff} of SPP mode is good, due to the SSP mode and core mode the phase matching condition, the wavelength shifted, and projected energy of spectrum intensity is changing.

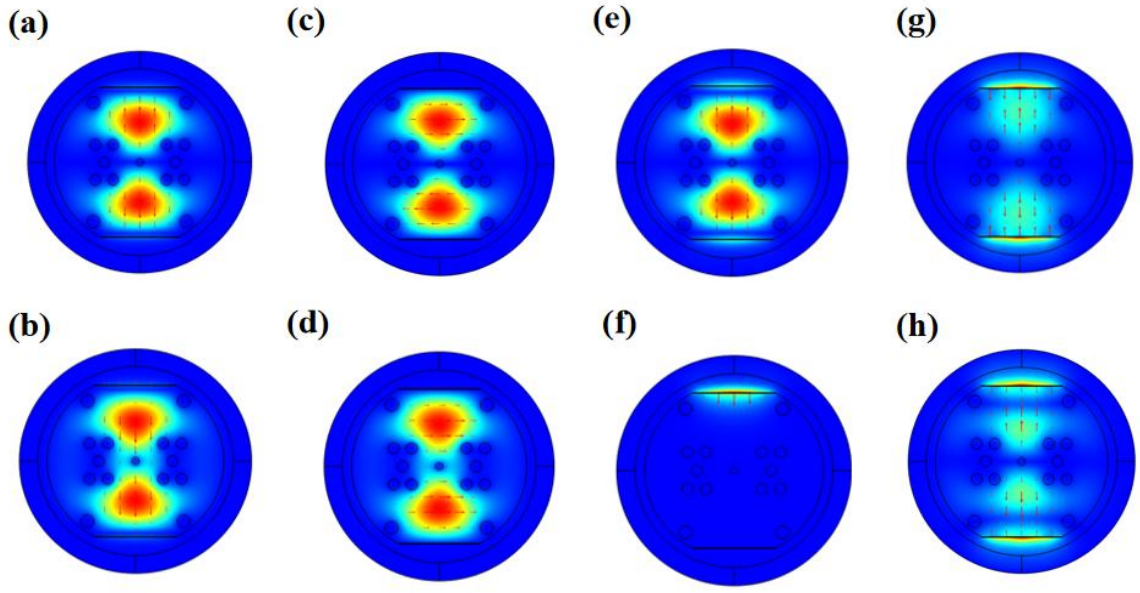
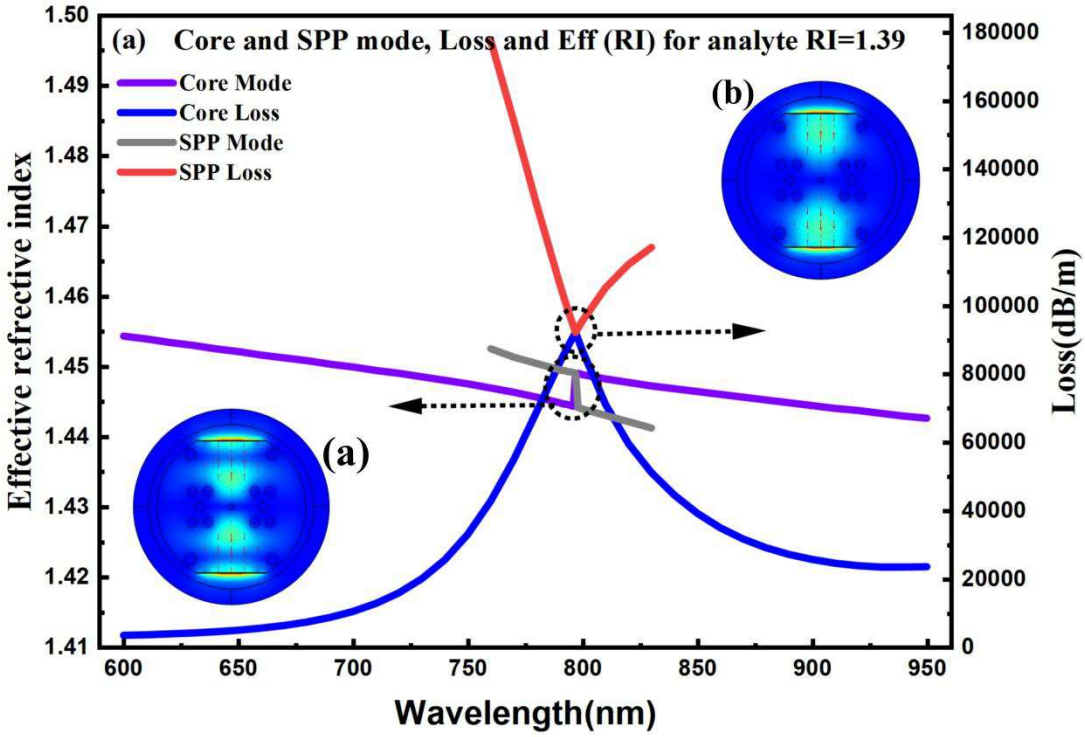


Figure.2 Electric field distribution. (a) Y-P odd core mode, (b) Y-P even core mode, (c) X-P odd core mode and (d) X-P even core mode at the wavelength of 600 nm for analyte RI=1.40. (e) Y-P odd core-like mode and (f) cladding defect-like mode at the wavelength of 712 nm. (g) Y-P odd super core-like mode and (h) Y-P cladding defect like mode at the wavelength 885 nm.

In Figure 2, we see the distribution of the electric field for Y- Polarization odd, Y- Polarization even, X-Polarization odd and X- Polarization even of four super models. Fig. 2 (a), (b) show the first two models of Y-P (odd mode, even mode) and (c), (d) models of X-P (odd mode, even mode) at the wavelength 600 nm. This film deposition method showed the highest value of Y-P loss in the vertical direction. The loss peaks of X-polarization are very small compared to Y polarization due to the design of the sensor. The designed sensor exhibits greater loss and resonant wavelength shift in Y-P mode, requiring further simulation. When the wavelength is short, around 600 nm, the light is entirely located within the fiber core, and there is not present light in the cladding. As the wavelength increases to 712 nm, light leakage from the core to the cladding begins, as shown in Figures 2(e) and (f). when the wavelength going to increases, losse also increases, reaching a maximum at 885 nm. At this wavelength, the probability of light being transmitted from the core to the cladding defect mode is highest. Within this wavelength range, the two modes behave similarly, generating surface plasmon resonance (SPR) phenomena for analytes with a refractive index of 1.40, as shown in Figures 2 (g) super core-like mode and (h) defect cladding-like mode. From the core-like mode, maximum energy is transferred to the cladding defect-like mode, and the SPR surface plasmon resonance phenomenon occurs for RI 1.40 and also for analyte 1.39 at wavelength 797 nm. Our design ensures stable performance and reliable resonance transitions, enabling the measurement of the refractive index of analytes 1.39 and 1.40 with highly sensitive SPR detection.

Figure 3(a) representing the phase matching and SSP mode for Y-P odd mode. This is the relationship between the effective index and loss. In the figure (a), we see the core mode loss and the loss reaches a maximum, and the red color peaks are SSP loss goes to the minimum value. At wavelength 797 nm, both losses are interacting for analyte 1.39, Figure. 3(b)similarly for analyte 1.40 at the wavelength 885 nm. The narrow and sharp peaks show strong coupling theory for core and SSP modes. From the core mode, energy is transferred to the cladding defect-like mode. This phenomenon is said to be SPR. Inside the fiber, the light travels during the non-resonant wavelength at which it is observed.



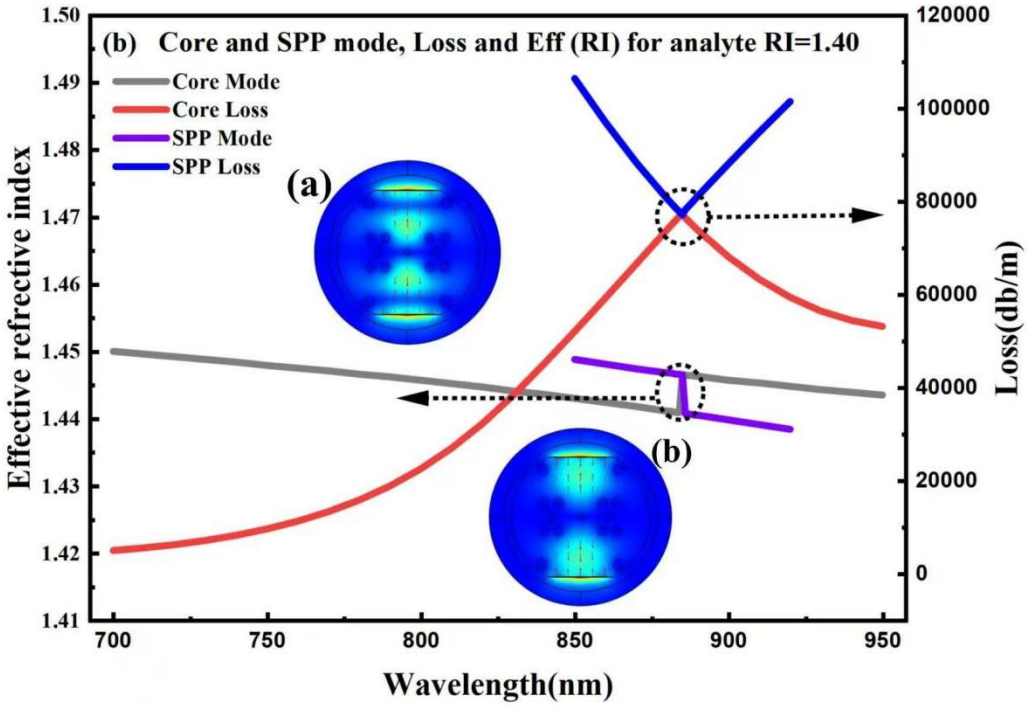


Figure. 3.(a) Effective RI ratio versus SPR phenomenon for Y-P odd mode, RI=1.39 at wavelength 797 nm. (a) and (b) represent the core- defect and cladding defect mode during SR phenomenon. **Fig.3** (b) for Y-P odd mode, RI=1.40 at wavelength 885 nm.

Based on detail of the study. Around the medium surface and the gold film, the SSP mode is distributed. SP is very sensitive to the dielectric to effective index RI. . The (n_{eff}) of Y-P SSP and core mode under the phase matching is equal. The core mode guided and (n_{eff}) very equal in the normal circumstances they are nearly similar to RI of the core material. Silica is similar to (n_{eff}) of SP, and air to gold. By observation of resonance wavelength or transmitting power during the duration of the spectra loss can easily identify the changes in RI for an analyte.

Results and discussion

Gold and silver comparison and its effect on sensor performance as plasmonic material

Figure 4 shows a comparison of Au versus Ag in the proposed sensor. To the SPR phenomenon, every material behaves differently. For a different purpose PCF sensor use different plasmonic material. A thickness of 40 nm is used for both gold and silver on the surface of the fiber deposited externally and keen for analytes 1.36, 1.37, and 1.38. As shown in the figure, different material has different wavelengths for the same analyte RI.

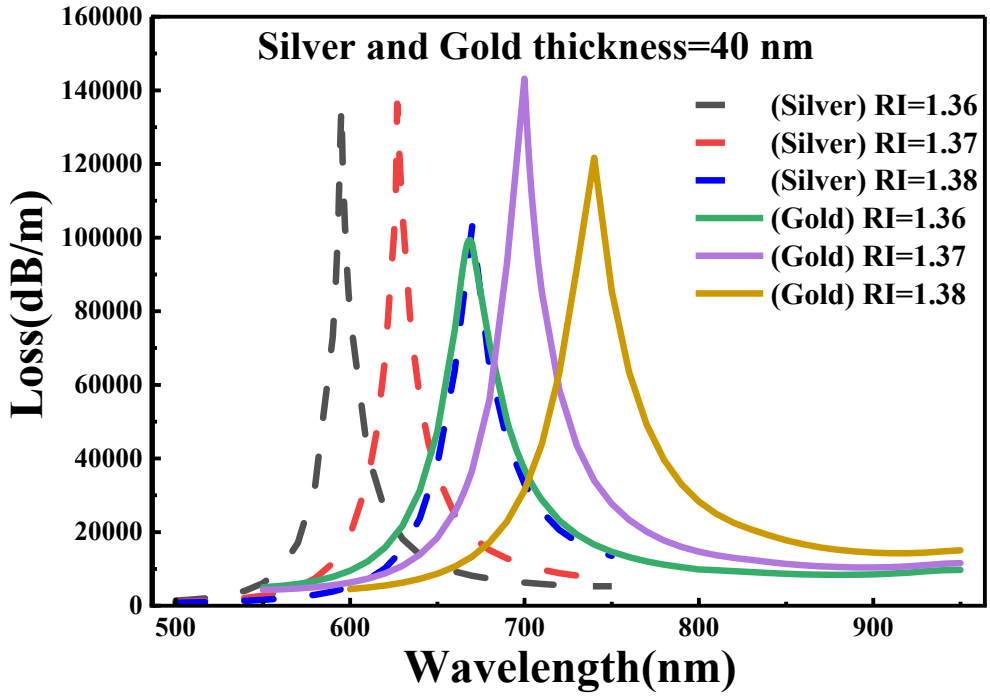


Figure.4 . Effective RI ratio versus SPR phenomenon for Y-P odd mode, RI=1.37 at wavelength 700 nm. (a) and (b) represent the core- defect and cladding defect mode during SR phenomenon.

The loss peak of gold (Au) is greater than that of silver (Ag) for the same RI 1.36 and so on. Au has a greater loss peak than Ag for equal RI, due to the different resonance wavelength, which is discussed in the above literature as well. As the analyte increases, the resonance wavelength shifts towards the longer wavelength. The figure shows this is good to use gold in the comparison of silver; the silver loss peak is greater than that of gold. In this case, we see the highest loss peak for both on gold is a higher peak due to a different resonant wavelength. Similarly for analyte 1.38. A narrow and high loss peak provide the accurate, precise measurement and a high value for well polarization and extinction ratio (ER). Gold is more sensitivity than silver; they rapidly oxidize in the air, which affects their sensibility affected. As compared to silver, they are more biocompatible and chemically stable [28], In the environment the very useful, used many times. To improve the execution and strong support of SPR phenomena, gold was deposited externally on a polished surface.

Comparison of simulation work using Super modes

n this portion, we are going to compare the four super modes. Fig 5. (a), (c) shows the Y-P and (b), (d) shows X-P there are two modes of y and x polarization: odd modes, even modes. These are assessed with the variation RI of the analyte 1.30-1.40. Gold material is deposited horizontally at the bottom and top with a thickness of 40 nm on the polished sides of PCF. In the literature, we study for Y-P or y-axis high outflow peak as reported [29]. We observed that the core mode and SSP mode in Y-P coincide, causing less than horizontally than vertical axis. In figure (a) and (c) show the confinement loss for the analyte range 1.30 to 1.40 with the wavelength. From 1.30 to 1.37, the (CL) confinement losses increase and are sharpest. The highest losses peak is 143160 dBcm^{-1} obtained at 1.37 at 700 nm wavelength. After this peak or 1.37, the loss peak is going down, mean decreasing from 1.38 to 1.40 as compared to 1.37. The proposed sensor efficiently increases until 1.37, then decreases. In increase RI in response, displaying a red shift, the resonance wavelength shifts toward longer wavelengths. Between 1.39 and

1.40, the maximum resonance wavelength shifts are observed, and this indicate highest wavelength sensitivity.

In figures 5 (b) and (d), there are so many peaks of X-P even mode and X-P odd mode 820 nm to 920 nm resonance wavelength. Several X-P Loss peaks at different resonance wavelengths, 889, 899 and 920 nm are seen in Figure 5. The loss is less in X-P than in Y-P, the high peaks for X-P between 1.30-1.40, expected between 850 and 920 nm. At the resonance wavelength, the coupling is very small for X-P core mode and SSP mode. The X-P core mode and SSP modes have different coupling results. That's why the SPR phenomenon's result is very low for X-P even and odd modes.

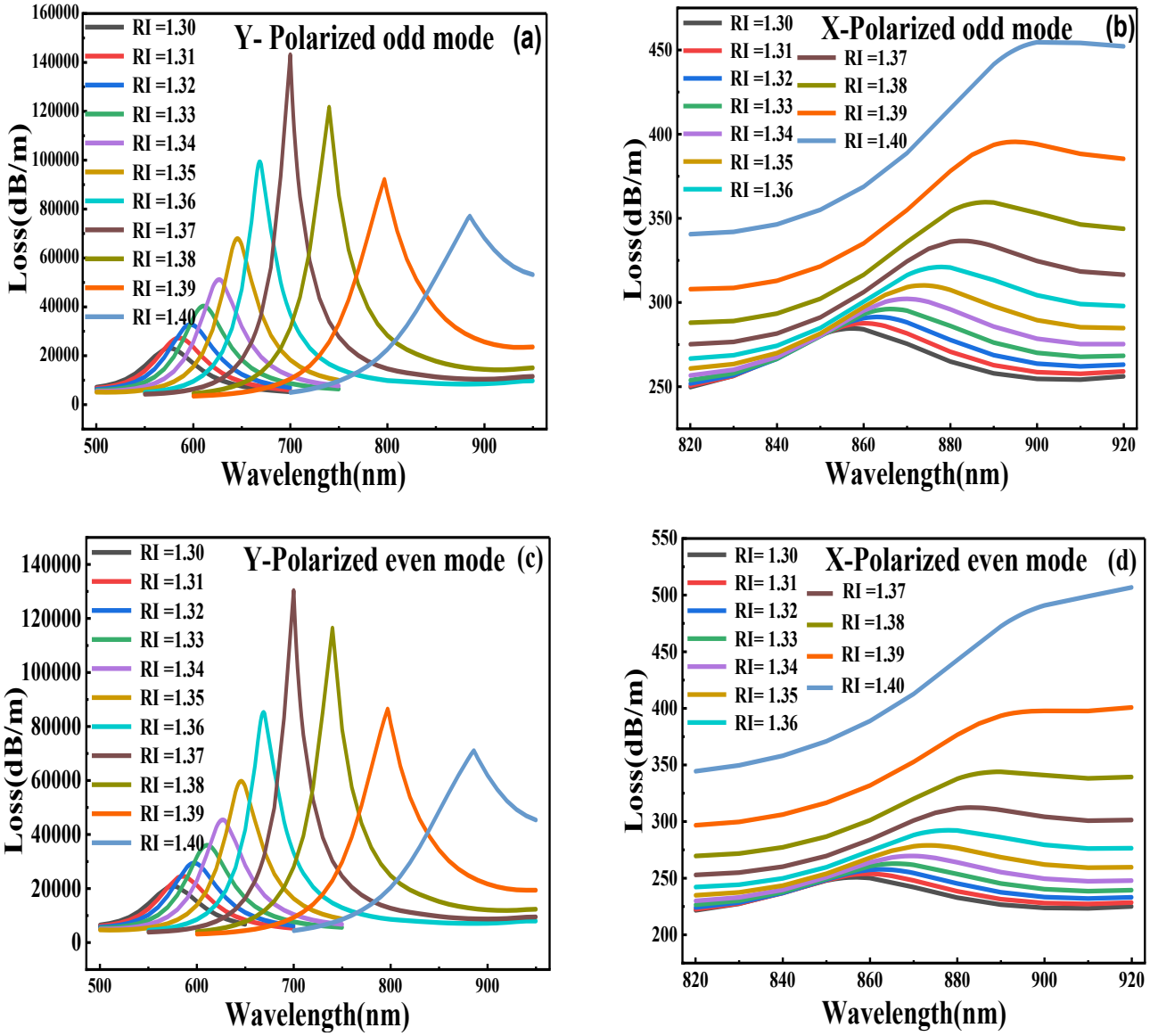


Figure. 5 Different super model wavelength versus confinement loss relation at different analytes range (1.30 to 1.40), Y-P odd mode (a) and Y- P even mode (c), X-P odd mode (b) and even mode (d).

Resolution performances and Sensitivity

Greater sensitivity provides accurate results, for better work precision and accurate is also counted in the sensors. For the evaluation of sensor capability, the main factor is the type of sensor. The wavelength sensitivity is calculated by the following formula.

$$S_W(\lambda) = \frac{\Delta \lambda_{peak}}{\Delta n_a} \qquad (4)$$

In the above equation $\Delta \lambda_{peak}$ and Δn_a represent changing in RI of the analyze and resonance peak shift. Figure. 6 (a) represents the wavelength sensitivity for different RI values in the range from 1.30 to 1.40. Our proposed sensor for analyte 1.30 shows 1000 nm/RIU, which is low sensitivity. As the analyte increases, the sensitivity of the proposed sensor increases. Maximum sensitivity 8800 nm/RIU is obtained between 1.39 and 1.40 RI.

Another important factor for sensor performance is Amplitude sensitivity; we can measure the amplitude using the interrogation method. Spectral manipulation is not required for this method, as compared to wavelength sensitivity, which is considered low. For the calculation using the formula.

$$S_A(\lambda) = \frac{1}{\alpha(\lambda, n_a)} \frac{\delta\alpha(\lambda, n_a)}{\delta n_a} \qquad (5)$$

The at resonance wavelength the (CL) peak is represented by $\alpha(\lambda, n_a)$,the adjacent analyte loss difference is denoted by $\delta\alpha(\lambda, n_a)$ and δn_a in Figure. 6 (b) represent RI changes between 1.30 to 1.40. The maximum amplitude sensitivity (AS) 286 RIU^{-1} is obtained for analyte 1.37. another important

parameter is the sensor resolution (SR) calculated as follows

Figure. 6 Shows for Y-P odd mode (a) Wavelength sensitivity for RI (1.30 – 1.40) and (b) amplitude Sensitivity for RI (1.30-1.40).

$$R(RI) = \frac{\Delta n_a \, \Delta \lambda_{min}}{\Delta \lambda_{peak}} \qquad (6)$$

'R' is used in the above equation for resolution, Δn_a is the symbol of adjoining for RI variation of analyze, spectrometer $\Delta \lambda_{min}$ minimum resolution for the adjacent loss of peaks of different resonant wavelength is $\Delta \lambda_{peak}$. In this study we used the $\Delta \lambda_{min}$=0.1 and Δn_a=0.01 are matched the spectrometer's actual resolution[30]. 1.13636×10^{-5} achieved the maximum spectral resolution[30] on the base of above equation.

Sensor performance and effect on structural parameters

Various structural parameters are utilized in the section to make sure the sensor performance more efficiently. Figure 7 (a) shows the loss versus wavelength for different polishing depths. The depth thickness calculated for 0.44, 0.54, 0.64 and 0.71 µm for analyte 1.40. The high loss for thickness 0.71 µm is 160540 dB/m, 0.64 µm is 155520 dB/m and for 0.44 µm is 143020 db/m. The figure shows that as the thickness increases proportionally, the losses increase minimally. And towards longer wavelength is resonance wavelength shifts because of red shift, of wavelength with increasing polished depth. For the manufacturing process, the most difficult work is to change the depth of polishing. With the increase in depth polishing, it is easy to make a coupling between the metal surface and the core mode due to the closeness of both. For theoretically and experimental reasons, it is important to control the depth of polishing. Therefore, the depth of polishing of 0.54 µm is considered optimal and utilized in the simulation.

Figure 7. (b) shows the variation of different PML that's how due to PML variation the sensor performance is affected due to PML variation. The difference is taken from 0.70 µm , 0.85 µm,1.0 µm, 1.3 µm and 1.5 µm, with almost negligible variation observed in very little friction. The figure of different PMLs does not affect the sensor performance.

Figure 7. (c) shows different gold thicknesses of 30 nm,40 nm and 50 nm for the same analyte 1.37. For better efficiency for sensor perform we deposited Au of different thickness [31]. The resonance wavelength is 635 to 645 nm for 30 nm for analyte 1.37. For a 40 nm thickness, the resonance wavelength is from 692 to 703 nm. Similarly, for a thickness of 50 nm.

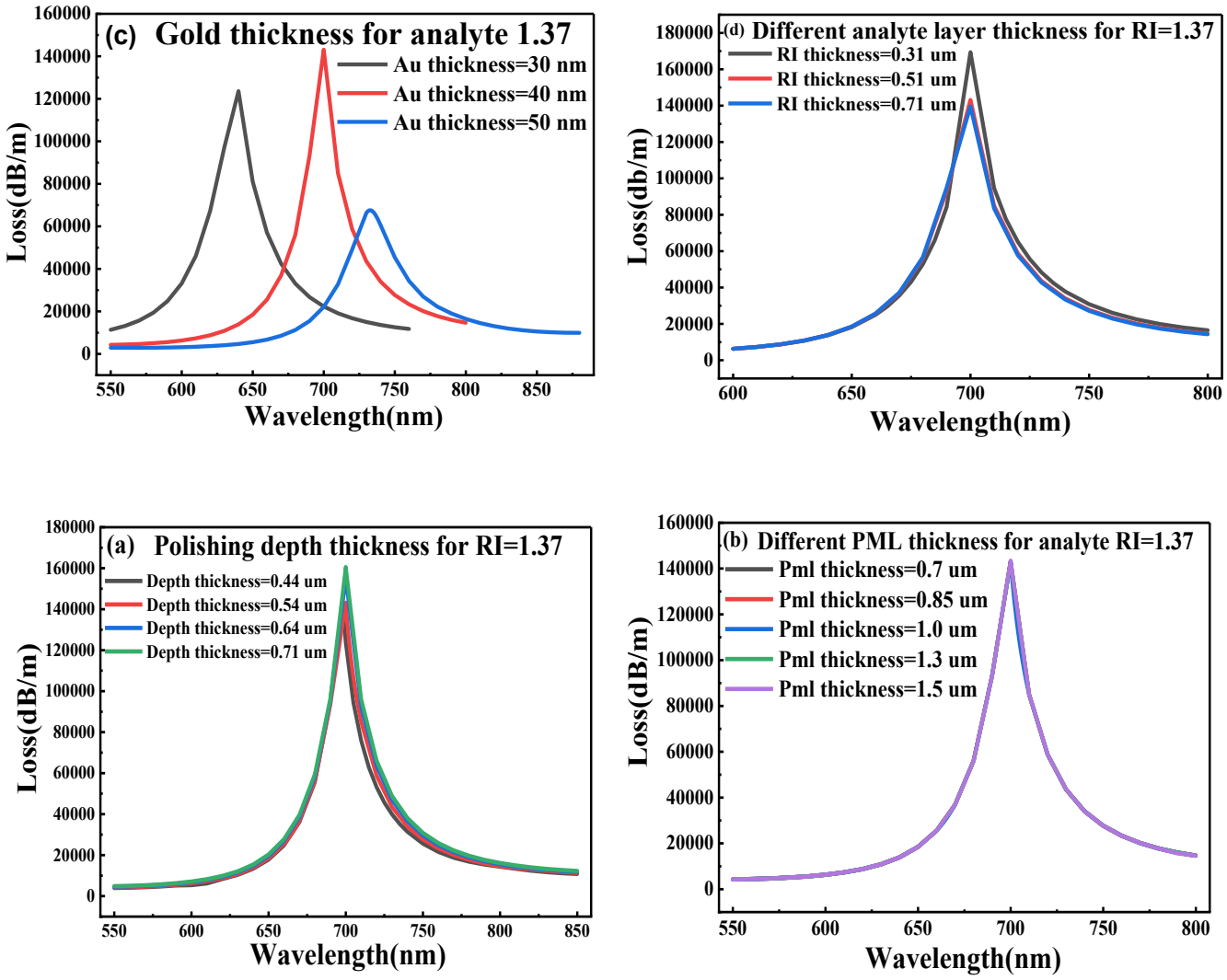


Figure 7. Confinement Loss for analyte RI (1.37) at a different (a) polishing depth (0.44, 0.54, 0.64 and 0.71 µm), (b) different PML layer thickness(0.7, 0.85, 1.0, 1.3 and 1.5 µm), (c) different Au thickness (30 ,40 and 50 nm) and (d) different Analyze thickness layer (0.31, 0.51 and 0.71 µm).

The resonance wavelength is from 666 to 672 nm, the loss peak is less than two, showing good sensitivity and acceptable for working in long-range RI and is expected to show better wavelength sensitivity. Resolution results also provide better results. The resonance wavelength shifts toward longer when the gold thickness is increased. A thin layer cannot support the SPR, while a thick layer can support it [32]. We considered 40 nm for the optimal thickness. Figure 7 (d) represents the various thicknesses 0.31 μm, 0.51 and 0.71 μm for analyte 1.37. When the analyte layer increases, the loss also increases and becomes narrower. Due to a decrease or increase in the layer, the resonance wavelength can be affected, as we seen the figure mean the sensitivity does not change for the proposed sensor. We have used 0.51 μm in our simulation. Our proposed model improved compared to [17-33].

Performance of polarization filtering for different fiber transfer lengths

In optical integrated the polarization filtering is playing important role. To improve and develop the sensor researcher work on it that capable of high accuracy and high polarization filtering. As we discussed, the large polarization peaks for Y-P and X-P Figure 6 shows the highest loss of Y-odd mode 143165 dB/m for analyte 1.37 at the at resonance wavelength 700 nm is calculated by the Sellmeier equation. In the literature this reported that the greater change between two polarization effects of polarization. Due to the proposed PCF silica, the silica material exhibits very high loss, so their losses can ignored as compare to PCF loss in during calculation of transferring power. P_{out}(x, y) can calculated by this equation.

$$P_{out}(\mathrm{x, y}) = P_{in}(x, y)\ e^{(-\alpha(x,y)(\frac{ln\,10}{10})\mathrm{L})} \qquad (7)$$

In the above equation $P_{in}(x,y)$= 1, $\alpha(x, y)$ L represent the input power, of transferring length and confinement loss.

The below formula calculates the extinction ratio;

$$\mathrm{ER} = 10\ log_{10}\frac{p_{out(y)}}{p_{out(x)}} \qquad (8)$$

In the extinction ratio formula $p_{out(y)}$ and $p_{out(x)}$ shows the out power in Y and X polarization. Figure 8 (a) showing the output power of Y-P odd mode while the (b) representing X-P odd mode output power. There are different transferring lengths the results obtain reduce the output power by increasing the transfer length. Sensor can realize better polarization extinction ratio (ER). The transferring of length of 2 mm achieve the (ER) extinction ratio is -65.85 dB at resonance wavelength 700 nm and is well

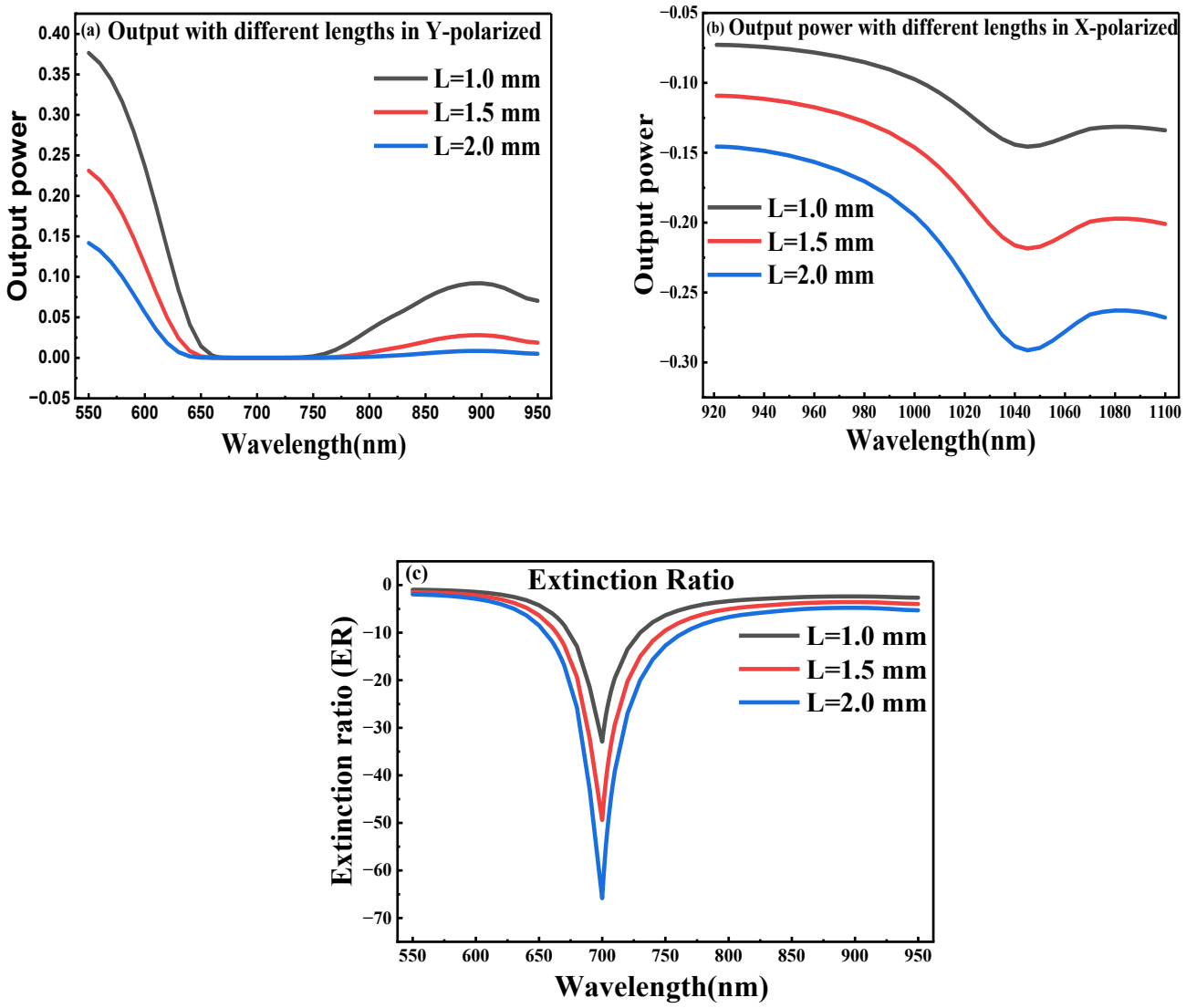


Figure 8. Output power for (a) Y-P direction ,(B) X-P direction and (c) Show the extinction ratio (ER).

Table 1. The performance of proposed sensor in terms resolution and sensitivity for (1.30-1.40).

RI	Resonance wavelength (nm)	Loss(dB/m)	RI Difference	Resonance wavelength shift (nm)	Sensitivity (nm/RIU)	Resolution (RIU)
1.30	575	23061	1.31-1.30	10	1000	1×10^{-4}
1.31	585	27212	1.32-1.31	11	1100	9.090×10^{-5}
1.32	597	32733	1.33-1.32	14	1400	7.14×10^{-5}
1.33	611	40284	1.34-1.33	16	1600	6.26×10^{-5}
1.34	672	51104	1.35-1.34	19	1900	5.26316×10^{-5}
1.35	646	67889	1.36-1.35	23	2300	4.34783×10^{-5}
1.36	669	99261	1.37-1.36	31	3100	3.2258×10^{-5}
1.37	700	143,160	1.38-1.37	40	4000	2.5×10^{-5}
1.38	740	121,680	1.39-1.38	57	5700	1.75439×10^{-5}
1.39	797	92131	1.40-1.39	88	8800	1.13636×10^{-5}
1.40	885	77118	NA	NA	NA	NA

Conclusion

A dual-function surface plasmon resonance system is proposed for RI sensing as well as polarization filtering in this study. With its simple structure, our sketched sensor shows better polarization and is capable of identifying a wider variety of RI. A plasmonic material and its thickness contribute to the superior performance of our sensor. This sensor's structure allows for externally-analyte sensing, making it easy to change the RI for different purposes. This sensor has a very simple, easy-to-fabricate design, low cost, and is affordable, even with limited resources. The high loss change between Y and X polarizations makes it suitable for polarization filtering. Based on the optimization of the structure, the maximum WS is 8800 nm/RIU in the RI range of 1.30-1.40. The maximum confinement loss measured for Y-polarization is 143,160 dB/m for an analyte with RI=1.37. The extinction ratio is -65.85 for polarization filter effects. Spectral wavelength resolution of $1.13636\times10^{-5}$and the amplitude sensitivity (AS) 286 RIU^{-1}. With a wide range of RI, it can be used for biological sensing, and chemical sensing as well as polarization filtering.

Contributions All coauthors contributed significantly to the work presented in this article. conceptualization and design of the work: Jawad Khan; writing of the manuscript: Jawad Khan and Hailing chen; Formal analysis and supervision Hailing Chen; Writing comments and suggestions: Hailing Chen.

Funding This work was supported by the National Natural Science Foundation of China (Grant No. 12074331) and Natural Science Foundation of Hebei Province, China (Grant No. F2021203112).

Data availability the data support the findings of the study are available upon reasonable request from the authors.

Declarations

Ethics Approval Not applicable

Consent to participate All authors agree to participate in this investigation

Consent for publication All authors agree to participate in this article

References

1. Ullah, S., et al., *Dual-side polished surface plasmon resonance–based photonic crystal fiber for refractive index sensing and polarization filtering.* 2024. **19**(5): p. 2615-2625.
2. Ortega-Mendoza, J.G., et al., *Optical Fiber Sensor Based on Localized Surface Plasmon Resonance Using Silver Nanoparticles Photodeposited on the Optical Fiber End.* 2014. **14**(10): p. 18701-18710.
3. Weng, S., et al., *High sensitivity side-hole fiber magnetic field sensor based on surface plasmon resonance.* 2016. **14**(11): p. 110603.
4. Liu, C., et al., *Near-infrared surface plasmon resonance sensor based on photonic crystal fiber with big open rings.* Optik, 2020. **207**: p. 164466.
5. Pandey, P.S., S.K. Raghuwanshi, and S.J.I.S.J. Kumar, *Recent advances in two-dimensional materials-based Kretschmann configuration for SPR sensors: A review.* 2021. **22**(2): p. 1069-1080.
6. Rizal, C. and V.J.T.E.P.J.P. Belotelov, *Sensitivity comparison of surface plasmon resonance (SPR) and magneto-optic SPR biosensors.* 2019. **134**(9): p. 435.
7. Liu, Y. and H. Chen, *First- and second-order SPP-mode co-induced dual-polarized refractive-index sensor based on photonic crystal fiber and gold film.* 2021. **54**: p. 325103.
8. Winzer, P.J., D.T. Neilson, and A.R.J.O.e. Chraplyvy, *Fiber-optic transmission and networking: the previous 20 and the next 20 years.* 2018. **26**(18): p. 24190-24239.

9. Elsherif, M., et al., *Optical fiber sensors: Working principle, applications, and limitations.* 2022. **3**(11): p. 2100371.
10. Hameed, M.F.O., et al. *Novel multichannel surface plasmon resonance photonic crystal fiber biosensor*. in *Optical Sensing and Detection IV*. 2016. SPIE.
11. Han, J., E. Liu, and J.J.J.o.t.O.S.o.A.A. Liu, *Circular gradient-diameter photonic crystal fiber with large mode area and low bending loss.* 2019. **36**(4): p. 533-539.
12. Mandal, P.J.P., *Application of plasmonics in solar cell efficiency improvement: a brief review on recent progress.* 2022. **17**(3): p. 1247-1267.
13. Haider, F., et al., *Multi-analyte detection based on integrated internal and external sensing approach.* 2021. **21**(1): p. 29-36.
14. Liu, W., et al., *Surface plasmon resonance sensor composed of microstructured optical fibers for monitoring of external and internal environments in biological and environmental sensing.* 2023. **47**: p. 106365.
15. Xue, J., et al., *Polarization filter characters of the gold-coated and the liquid filled photonic crystal fiber based on surface plasmon resonance.* 2013. **21**(11): p. 13733-13740.
16. Liu, C., et al., *Surface plasmon resonance (SPR) infrared sensor based on D-shape photonic crystal fibers with ITO coatings.* 2020. **464**: p. 125496.
17. Liu, Y., et al., *Surface plasmon resonance induced high sensitivity temperature and refractive index sensor based on evanescent field enhanced photonic crystal fiber.* 2019. **38**(4): p. 919-928.
18. An, G., et al., *Metal oxide-graphene-based quasi-D-shaped optical fiber plasmonic biosensor.* 2017. **9**(4): p. 1-9.
19. Rifat, A.A., et al., *Photonic crystal fiber-based surface plasmon resonance sensor with selective analyte channels and graphene-silver deposited core.* 2015. **15**(5): p. 11499-11510.
20. Zakaria, R., et al., *Fabrication and simulation studies on D-shaped optical fiber sensor via surface plasmon resonance.* Journal of Modern Optics, 2017. **64**(14): p. 1443-1449.
21. Teng, C., et al., *Investigation of U-shape tapered plastic optical fibers based surface plasmon resonance sensor for RI sensing.* Optik, 2022. **251**: p. 168461.
22. Ren, Q., et al., *Dual-band D-shaped SPR fiber sensor based on birefringence analysis.* Optics Communications, 2022. **506**: p. 127545.
23. Zeng, W., Q. Wang, and L. Xu, *Plasmonic refractive index sensor based on D-shaped photonic crystal fiber for wider range of refractive index detection.* Optik, 2020. **223**: p. 165463.
24. Lu, J., et al., *D-shaped photonic crystal fiber plasmonic refractive index sensor based on gold grating.* 2018. **57**(19): p. 5268-5272.
25. Chen, H., et al., *Ultrabroad bandwidth polarization filter based on D-shaped photonic crystal fibers with gold film.* 2015. **10**(5): p. 1239-1242.
26. Zhang, S., et al., *A wide measurement range plasmonic refractive index sensor based on side-polished photonic crystal fiber.* 2023. **98**(11): p. 115513.
27. Yu, Y.-L., et al., *D-shaped silicon core fiber-based surface plasmon-resonance refractive index sensor in 2 μm.* Applied Optics, 2020. **59**(18): p. 5539-5546.
28. Liu, Y., et al., *Surface Plasmon Resonance Induced High Sensitivity Temperature and Refractive Index Sensor Based on Evanescent Field Enhanced Photonic Crystal Fiber.* Journal of Lightwave Technology, 2020. **38**(4): p. 919-928.
29. Yan, J., et al., *Optical fiber sensor based on magneto-optical surface plasmon resonance with ultra-high figure of merit.* 2024. **99**(8): p. 085550.
30. Yin, Z., et al., *A broadband SPR dual-channel sensor based on a PCF coated with sodium-silver for refractive index and temperature measurement.* 2022. **41**: p. 105943.
31. Rifat, A.A., et al., *Highly sensitive D-shaped photonic crystal fiber-based plasmonic biosensor in visible to near-IR.* 2017. **17**(9): p. 2776-2783.
32. Duan, L., et al., *Hollow-fiber-based surface plasmon resonance sensor with large refractive index detection range and high linearity.* 2017. **56**(36): p. 9907-9912.
33. Hameed, M.F., et al., *Novel multichannel surface plasmon resonance photonic crystal fiber biosensor*. SPIE Photonics Europe. Vol. 9899. 2016: SPIE.